Application of an Advanced Repetitive Controller to Mitigate Harmonics in MMC With APOD Scheme

Sreedhar Madichetty, Abhijit Dasgupta, *Member, IEEE*, Sambeet Mishra, *Student Member, IEEE*, Chinmoy Kumar Panigrahi, and Ghouse Basha

***Abstract*—In a modular multilevel converter (MMC), the second and other even-order harmonics in the circulating currents are mainly due to the fluctuations in the capacitor voltages in the sub modules of the MMC. The increased circulating currents affect the system performance and threatens the safety operation of power devices. To mitigate the circulating currents, this article puts forward the application of an advanced repetitive controller with alternate phase opposition and disposition pulse-width modulation technique. The proposed controller was operated in tandem with a proportional integral controller for better results of circulating current harmonic suppression and then the stability analysis was analyzed by the Popov criteria. This method is very simple to implement and suitable for multiple harmonic mitigation. Computer simulations and experimental results on a prototype shows that the proposed controller is effective and easy to implement for MMCs.**

***Index Terms*—Harmonic mitigation, MMC dynamics, MMC stability, modular multilevel converter.**

I. Introduction

THE field of MMCs has witnessed many rigorous investigations leading to successful operation in high voltage direct current (HVDC) systems. In recent times, very long distance HVDC transmission lines based on current source converters and voltage source converters (VSCs) have been used offering more economic and cost-effective power transmission. However, the HVDC transmission systems based on VSCs have been bestowed with warm-welcome owing to the manifold opportunities like the grid access of weak alternating current (AC) networks and independent control of the active and reactive power. In particular, the novel power converter topology for MMCs has been intensively researched and developed, and then, was evaluated for many features like high modularity, simple scalability, robust control, and redundancy. MMC is composed of identical sub modules (SM) connected in series, each one built up with standard components, enabling the connection to high-voltage poles. Although the MMCs and derived topologies offer several advantages, they also introduce a more complex design of the power circuit and control goals, which are the main reasons for the recent ongoing research. Furthermore, medium voltage VSC's are an interesting area for the application of MMCs .The ever increasing demand of industry for stability, adaptability and accuracy of control of power electronic (PE) equipment at very high voltages led to the development of relatively less total harmonic distortion (THD) based modern PE static converters. PE converters produce complex waveforms, which can be resolved into a series of sinusoidal waves of various frequencies. Hence, any complex waveform is the sum of a number of odd and/or even harmonics, which can be eliminated by designing a proper controller by tuning it in to unwanted harmonic components.

Due to the uneven voltage distribution in the legs of MMCs, circulating currents flow through the legs of the converter. It consists of second and even-order current harmonics resulting in the deterioration of the system performance. To control and mitigate the harmonics, in [1], a method has been proposed under balanced voltage condition; in which the circulating currents have been suppressed with an inner current controller. A method based on nonideal proportional resonant controller has been implemented in [2]. This [2] controller is designed in stationary α, β reference frame and well adopted for variation in grid frequencies. This [2] method has a disadvantage in that the ac side current must be separated into the positive and negative sequences for control under an unbalanced voltage condition. To overcome this disadvantage, an enhanced control method has been implemented without separating the positive and negative sequence components [3]. To control the voltage oscillations, an energy-based controller has been proposed in [4]. This technique has a disadvantage of not controlling the circulating currents in the converter. A conventional technique based on theoretical relationship between switching frequency and circulating current has been developed in [5]. This [5] technique has several disadvantages for not controlling at unbalanced conditions. A technique based on reduced switching frequency has been implemented in [6]. This control technique has the disadvantage of inclusion of a double-line-frequency ripple in ac-side active power by controlling ac-side negative-sequence currents to zero under unbalanced voltage conditions. A control method has been developed in, [17], [18], for circulating currents with inner current suppressing control in *a-b-c* stationary frame, since circulating currents have positive, negative, and zero sequence components under unbalanced voltage conditions. But, this method has the disadvantage of generating a phase delay because of its utilization of a high-pass filter to separate circulating currents; furthermore, it cannot improve the transient response occurring

Manuscript received September 11, 2014; revised June 15, 2015, July 25, 2015, and September 15, 2015; accepted November 2, 2015. Date of publication November 17, 2015; date of current version March 25, 2016. Recommended for publication by Associate Editor P. Barbosa.

S. Madichetty is with the Department of Electrical and Electronics Engineering, Birla Institute of Technology and Science Pilani, Pilani 333031, Rajasthan, India (e-mail: sreedhar.803@gmail.com).

A. Dasgupta and C. K. Panigrahi are with the Department of Electrical Engineering, KIIT University, Bhubaneshwar 751024, Odisha, India (e-mail: dg.abhijit@gmail.com; panigrahichinmoy@gmail.com).

S. Mishra is with Department of Electrical Engineering, Tallin Technical University, Tallin 10143, Estonia (e-mail: sambeets@gmail.com).

G. Basha is with Annamacharya Institute of Technology and Sciences, Kadapa, Andhra Pradesh, India (e-mail: munnaa209@gmail.com).

Color versions of one or more of the figures in this paper are available online at http://ieeexplore.ieee.org.

Digital Object Identifier 10.1109/TPEL.2015.2501314

in the inner unbalanced currents and dc-link currents under unbalanced voltage conditions. A selective harmonic elimination-based technique has been implemented in [8] to eliminate the voltage harmonics at the output terminals of the MMC. A carrier phase shift based PWM has been implemented in [9] with a plug-in repetitive controller. However, this method [9] has a disadvantage in the calculation volume of the processor, which increases with an increase in the level of the MMC. The steady-state analysis of the converter has been given in [10], which gives a clear idea about MMC in steady state and simplified terminal behavior model has been presented in [12]. A repetitive control [11] scheme has been implemented by converting the controller into discrete form. It has various advantages but is slow under transient [21]. The various repetitive controllers have witnessed excellent characteristics in various applications [14], [15], [20] especially in wind power systems. The various stability analysis for different controllers have been given in [13]. Different capacitor voltage balancing schemes have been proposed to control the circulating currents. But the main disadvantage is that it exhibits sluggish response under transient conditions and also require many voltage sensors which increases the cost of the system. The different balancing schemes have been proposed in [16] and [19]. To overcome the above drawbacks, this article presents an advanced repetitive controller in a closed-loop method for suppression of multiple harmonic currents. To improve the transient response, the proposed controller is paralleled by the proportional integral controller. This method is very simple to implement and applicable to single-phase and three-phase system applications in the HVDC transmission system and FACTS applications like static synchronous compensator, etc. The APOD-PWM scheme has been applied, while the balancing of SMs capacitor voltage is not affected. The proposed controller stability is analyzed by the Popov criteria. Verification results shows that this method can suppress the circulating currents and its transient response substantially compared with the existing methods [7], [11].

This paper is organized in five sections. In Section I, it provides the introduction about the MMC with the literature overview; Section II provides modeling of MMC in state-space approach; In Section III the controller design has been elaborated with its stability analysis by Popov approach, Section IV provides simulation and experimental verification; and finally the discussion and conclusion.

II. Mathematical Modelling of Circulating Currents

The basic circuit topology is shown in Fig. 1. It is a three-phase N-level MMC having n SMs in the upper arm and n SMs in the lower arm. This circuit mainly consists of an inductor having self-inductance $L1$ and $L2$, also called as arm inductors denoted by L and these are present in each leg of the converter. Each module consists of SM switches $S1$ and $S2$ with their antiparallel diodes $D1$ and $D2$, respectively as shown in Fig. 1. SM switches $S1$ and $S2$ consist of a capacitor, connected in parallel and it is denoted as $Cs1$.The basic switching operations for some operating states has been shown in [1]. The top SM switches in R phase upper leg are considered as $S1, S2, S3..Sn$ and the lower leg are considered

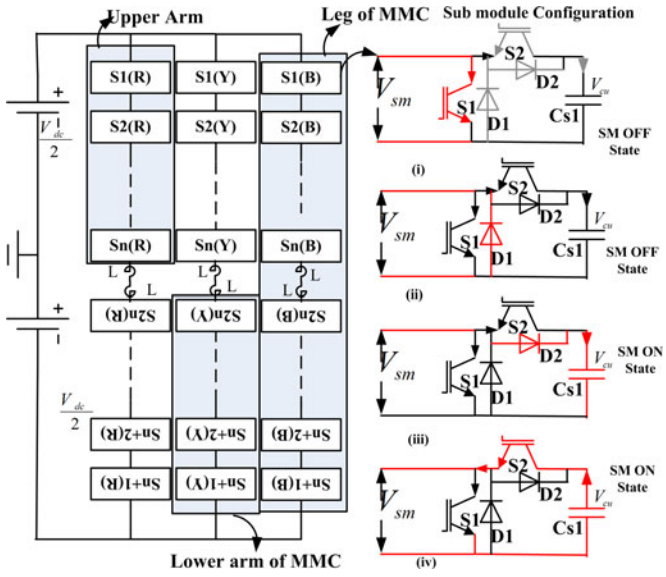

Fig. 1. Three-phase N-level MMC with SM operation.

as $S(n+1), S(n+2), S(n+3) \ldots, S(2n)$. The instantaneous voltages across the capacitors in the SMs are denoted as V_{c1}, $V_{c2} \ldots V_{cn}$. The current flowing through the R phase upper leg, bottom leg, circulating current, and phase currents are represented by $I_{tR}, I_{lR}, I_{cirR}, I_R$, respectively. Kirchoffs voltage law (KVL) has been applied to find the voltage across R phase and represented as V_{tR} for upper arm and V_{lR} for lower arm. The input supply voltage is $V_{\rm dc}$. Initially, it is assumed that the voltage across all SM capacitors in upper arm and lower arm are equal and shown in (1) and (2), respectively

$$V_{c1} = V_{c2} = V_{c3} \cdots = V_{cn} \tag{1}$$

$$V_{n+1} = V_{c(n+2)} = V_{c(n+3)} \cdots = V_{c(2n).} \tag{2}$$

Under any switching condition, the sum of capacitors voltage for upper arm $\sum V_{cu}$ and lower arm $\sum V_{cl}$ is shown in (3) and (4), respectively. The voltage across the SM capacitors may change mainly due to switching action of SMs. The sum of differential capacitor voltage for upper arm $\sum \Delta V_{cu}$ and lower arm $\sum \Delta V_{cl}$ can be written as shown in (5) and (6), respectively. The average voltage across each upper arm SM and each lower arm SM can be written as shown in (7) and (8), respectively, with input dc voltage as $V_{\rm dc}$

$$\sum V_{cu} = V_{c1} + V_{c2} \cdots + V_{cn} \tag{3}$$

$$\sum V_{c1} = V_{c(n+1)} + V_{c(n+2)} \cdots + V_{c(2n)} \tag{4}$$

$$\sum \Delta V_{cu} = \Delta V_{c1} + \Delta V_{c2} \cdots + \Delta V_{cn} \tag{5}$$

$$\sum \Delta V_{c1} = \Delta V_{c(n+1)} + \Delta V_{c(n+2)} \cdots + \Delta V_{c(2n)} \tag{6}$$

$$\frac{\sum V_{cu}}{N} = \frac{V_{\rm dc} + \sum \Delta V_{cu}}{N} \tag{7}$$

$$\frac{\sum V_{cl}}{N} = \frac{V_{\rm dc} + \sum \Delta V_{cl}}{N}. \tag{8}$$

From Fig. 1, the MMC has been modeled and its equivalent circuit shown in Fig. 2. The switching vector obtained by the

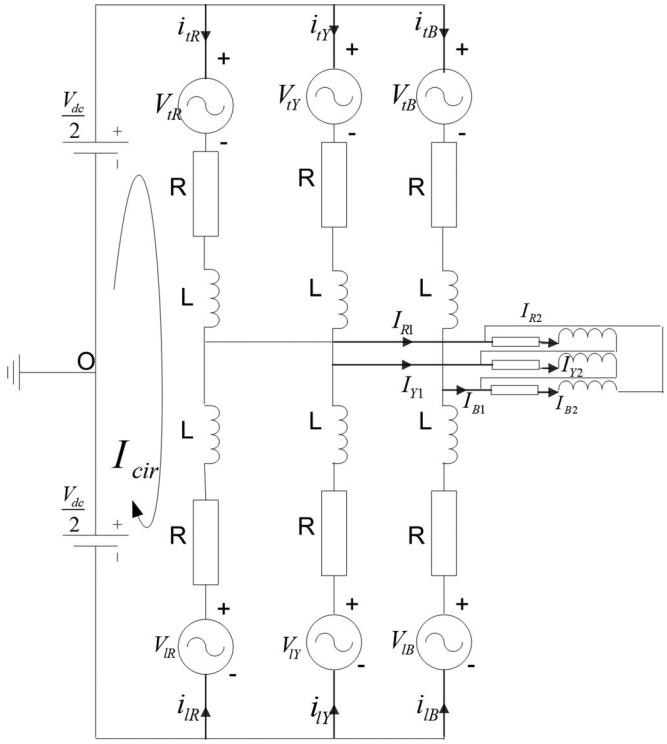

Fig. 2. Three-phase *N*-level equivalent circuit of the MMC.

alternate phase opposition disposition (APOD) scheme (which will be discussed in Section III) of R-phase upper arm can be written as in (11) as S_R and its conjugate can be written as shown in (12) as $\bar{S}_R$. The SM output voltage V_sm is obtained by the condition of the switch. If S_1 is OFF and S_2 is ON, its output voltage is shown in (9) and if S_1 is ON and S_2 is OFF, its output equation is shown in (10) with its operating modes shown in Fig. 1(i)–(iv)

$$V_{sm} = V_{cu} \tag{9}$$

$$V_{sm} = 0. \tag{10}$$

This modes of operation are called direct current flow and inverse current flow, respectively

$$S_R = [S_{m1}, S_{m2} \dots S_{mn}] \tag{11}$$

$$\bar{S}_R = [S_{n+1}, S_{n+2} \dots S_{2n}] \tag{12}$$

$$S_R + \bar{S}_R = N \tag{13}$$

where, S_R is the switching vector for the R-phase upper arm, which consists of all switching conditions of each SM and $\bar{S}_R$ is the switching vector for the R-phase lower arm. The sum of S_R and $\bar{S}_R$ is equal to *N* as shown in (13). Since at any point of time, *N* SMs will conduct in the leg of converter and necessary precautions should be taken not to operate the two switches in an SM at a time. The same conditions shall be applicable to Y and B phases as well. The output voltage at the terminals of the MMC (before connecting the load is denoted with suffix 1 and after connecting the load it is denoted with suffix $'2$ in equations) in terms of switching function can be written as (14), (15), and (16), where V_{R1}, V_{Y1}, V_{B1} represents the voltage across the R phase, Y phase and B phase, respectively, before connecting the load

$$V_{R1} = \frac{2}{3}[[2S_R - S_Y - S_B]V_{\text{in}} \tag{14}$$

$$V_{Y1} = \frac{2}{3}[-S_R + 2S_Y - S_B]V_{\text{in}} \tag{15}$$

$$V_{B1} = \frac{2}{3}[-S_R - S_Y + 2S_B]V_{\text{in}}. \tag{16}$$

By referring the equivalent circuit shown in Fig. 2, the current passing through the R phase (in *a-b-c* form) can be written as shown in (18) and for Y phase and B phase can be written as (19), (20), respectively. In this article, the internal resistance of each SM has been considered for respective capacitors and arm inductors as r_c1 and r_L1, respectively. For simplicity in writing, the matrix values have been denoted as different equations

$$\frac{r_{L1} + r_{c1}}{L_1} = W_1, \frac{r_{c1}}{L_1} = X_1, \frac{1}{L_1} = Z_1, \frac{r_{L1} + r_{c1}}{L_1} = W_2, \frac{r_{RL} + 2r_{c1}}{L_1} = X_2, \frac{1}{L1}\left(\frac{r_{c1}}{L_1} + \frac{r_{c1}}{L_R} = Z_2\right) \tag{17}$$

where I_R1, I_R2 is current passing through R-phase MMC before connecting to the load and after connecting to load respectively and V_R1 is the voltage across R-phase MMC

$$\frac{\mathrm{d}}{\mathrm{d}t}{I_{R1}}^a = -(W_1){I_{R1}}^a - (X_1){I_{R2}}^a - \frac{1}{L_1}{V_{R1}}^a + \frac{2}{3}[2S_R - S_Y - S_B]V_{\text{dc}} \tag{18}$$

$$\frac{\mathrm{d}}{\mathrm{d}t}{I_{Y1}}^b = -(W_1){I_{Y1}}^b - (X_1){I_{Y2}}^b - \frac{1}{L_1}{V_{Y1}}^b + \frac{2}{3}[-S_R + 2S_Y - S_B]V_{\text{dc}} \tag{19}$$

$$\frac{\mathrm{d}}{\mathrm{d}t}{I_{B1}}^c = -(W_1){I_{B1}}^c - (X_1){I_{B2}}^c - \frac{1}{L_1}{V_{B1}}^c + \frac{2}{3}[-S_R - S_Y + S_B]V_{\text{dc}} \tag{20}$$

where I_{R1}, I_{R2} is current passing through R-phase MMC before connecting to the load and after connecting to load, respectively, and V_R1 is the voltage across R-phase MMC

$$\frac{\mathrm{d}}{\mathrm{d}t}\begin{bmatrix} I_{R1}^a \\ {I_{Y1}}^b \\ {I_{B1}}^c \end{bmatrix} = \begin{bmatrix} -W_1 & 0 & 0 \\ 0 & -W_1 & 0 \\ 0 & 0 & -W_1 \end{bmatrix}\begin{bmatrix} I_{R1}^a \\ {I_{Y1}}^b \\ {I_{B1}}^c \end{bmatrix} + \begin{bmatrix} -X_1 & 0 & 0 \\ 0 & -X_1 & 0 \\ 0 & 0 & -X_1 \end{bmatrix}\begin{bmatrix} I_{R2}^a \\ {I_{Y2}}^b \\ {I_{B2}}^c \end{bmatrix} + \begin{bmatrix} -Z_1 & 0 & 0 \\ 0 & -Z_1 & 0 \\ 0 & 0 & -Z_1 \end{bmatrix}\begin{bmatrix} V_{R1}^a \\ {V_{Y1}}^b \\ {V_{B1}}^c \end{bmatrix} + \begin{bmatrix} \frac{2}{3}[2S_R - S_Y - S_B]V_{\text{dc}} \\ \frac{2}{3}[-S_R + 2S_Y - S_B]V_{\text{dc}} \\ \frac{2}{3}[-S_R - S_Y + 2S_B]V_{\text{dc}} \end{bmatrix}. \tag{21}$$

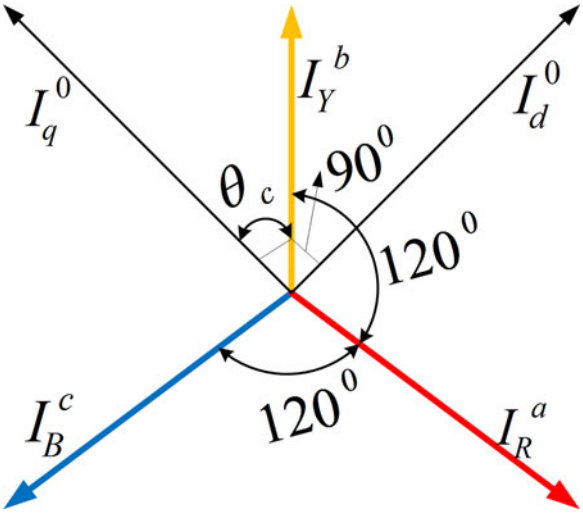

Fig. 3. *a-b-c* to *d–q* by using $parks$ transformation technique.

In the similar manner, the current passing through the load can be written as (21), where L_R is the load inductance and r_{RL} load resistance

$$\frac{\mathrm{d}}{\mathrm{d}t}\begin{bmatrix} I_{R2}^{a} \\ {I_{Y2}}^{b} \\ {I_{B2}}^{c} \end{bmatrix} = \begin{bmatrix} -W_1 & 0 & 0 \\ 0 & -W_1 & 0 \\ 0 & 0 & -W_1 \end{bmatrix}\begin{bmatrix} I_{R1}^{a} \\ {I_{Y1}}^{b} \\ {I_{B1}}^{c} \end{bmatrix} + \begin{bmatrix} -X_1 & 0 & 0 \\ 0 & -X_1 & 0 \\ 0 & 0 & -X_1 \end{bmatrix}\begin{bmatrix} V_{R1}^{a} \\ {V_{Y1}}^{b} \\ {V_{B1}}^{c} \end{bmatrix} + \begin{bmatrix} -Z_1 & 0 & 0 \\ 0 & -Z_1 & 0 \\ 0 & 0 & -Z_1 \end{bmatrix}\begin{bmatrix} V_{R1}^{a} \\ {V_{Y1}}^{b} \\ {V_{B1}}^{c} \end{bmatrix}. \quad (22)$$

For the simplicity in calculations, the obtained dynamic equations can be converted from *a-b-c* to d–q by using Park's transformation technique in Fig. 3.

The transformation could be thought of as a transformation from three axes to two axes; for uniqueness of the transformation, one set of axes to another set of axes, including the unbalance in the abc variables required three variable's such as $dq0$

$$\begin{bmatrix} I_q \\ I_d \\ I_0 \end{bmatrix} = \begin{bmatrix} \cos\theta_c & \cos\left(\theta_c - \frac{2\Pi}{3}\right) & \cos\left(\theta_c + \frac{2\Pi}{3}\right) \\ \sin\theta_c & \sin\left(\theta_c - \frac{2\Pi}{3}\right) & \sin\left(\theta_c + \frac{2\Pi}{3}\right) \\ \frac{1}{2} & \frac{1}{2} & \frac{1}{2} \end{bmatrix}\begin{bmatrix} I_R \\ I_Y \\ I_B \end{bmatrix}. \quad (23)$$

In a balanced three-phase MMC, the sum of the three-phase currents are zero and is given as $I_R + I_Y + I_B = 0$.

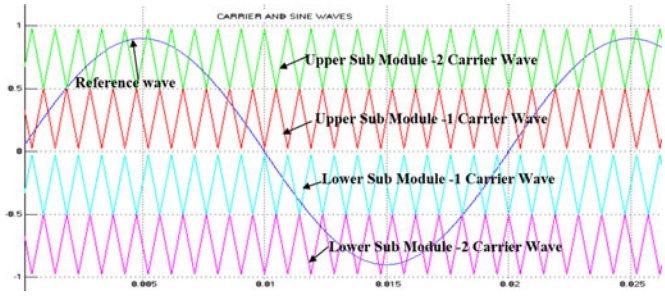

Fig. 4. APOD scheme for five-level MMC [*X*-axis time (S) and *Y*-axis amplitude (V)].

III. APOD PWM Technique and Design of Controller

A. APOD PWM Scheme

Due to its less complexity in generation of pulses for large number of switches, APOD pulse-width modulation (PWM) technique has been applied to MMC. For easy explanation, a five-level APOD scheme has been discussed and shown in Fig. 4. In this scheme, subsystem triangular wave generates four carrier waves of 1000 Hz frequency and these are compared with sine wave of 50 Hz frequency. Then the firing/gate pulses are generated to trigger the switches S_1, S_2, S_3, S_4 of Fig. 1. When these signals are passed through NOT logical operator then compliment signals are generated. Thus, obtained NOT signals are used to trigger lower arm switches of the MMC. Similarly 120 out of phase signals are used to trigger the rest of two arm switches. Switching scheme is followed according to Fig. 4. Complete information about APOD scheme can be found in [1]. Each leg of the MMC circuit consists of stacks of SMs and noncoupled buffer inductors. Each SM consists of a dc capacitor (floating) and IGBT's. By applying KVL to the loop of Fig. 2, which is independent of the load. The following equations could be obtained as shown in

$$V_{R0} = \frac{1}{2}\left(V_{tR} - V_{lR}\right) - \frac{1}{2}\left(L\frac{\mathrm{d}i_R}{\mathrm{d}t} + i_R \times R\right) \quad (24a)$$

$$2\left(\left(L\frac{\mathrm{d}i_{cirR}}{\mathrm{d}t} + Ri_{cirR}\right) = V_{\mathrm{dc}} - \left(V_{tR} + V_{lR}\right)\right. \quad (24b)$$

$$i_{cirR} = i_{tR} - \frac{i_R}{2} = i_{lR} + \frac{i_R}{2} \quad (24c)$$

$$i_{cirR} = \frac{1}{2}\left(i_{tR} = i_{lR}\right) \quad (24d)$$

where i_{cirR} is the *R*-phase circulating current. The relationship among the circulating current, the output current, and arm current could be written as shown in (24c) to (24d). The circulating current can be expressed in terms of fundamental components as shown in (24)

$$I_{cirR} = \frac{I_{\mathrm{in}}}{3} = \sum_{j=1}^{k} I_{acj}\sin\left(j\omega_0 t + \varphi_t\right) \quad (25)$$

where I_{in} is the input current, j is a positive integer varying from 1 to k, φ_t is the angle between voltage and current, and ω_0 is the angular frequency. The controller should be designed so as to be fully sufficed the (25). Further, by applying KVL to

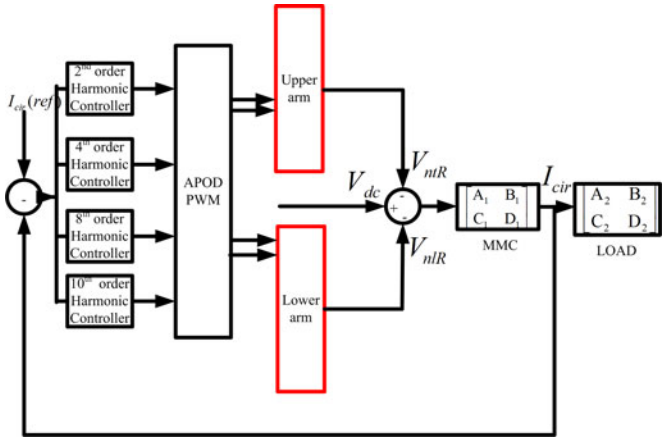

Fig. 5. Individual harmonic controller applied to the MMC.

Fig. 2, circulating currents in the upper leg and lower leg can be written as

$$I_{tR} = I_{\rm dc} + I_{R1} + \sum_{j=2}^{k} I_{acj} \sin\left(j\omega_0 t + \varphi_t\right) \tag{26}$$

$$I_{lR} = I_{\rm dc} - I_{R1} + \sum_{j=2}^{k} I_{acj} \sin\left(j\omega_0 t + \varphi_t\right). \tag{27}$$

From (26) and (27), it is evident that the upper and lower legs of converter consists even-order harmonic components. The designed controller should eliminate both the lower order and higher order even harmonics, since all odd harmonics are absent and evident as per (24). To efficiently eliminate the harmonics from the system, an individual controllers should be added as shown in Fig. 5. The second-order controller, fourth-order controller, sixth-order controller, eighth-order controller, and tenth-order controller have been added to remove the respective second, fourth, sixth, eighth, and tenth-order even harmonic components. Even though, the higher order harmonics are less in number, as the order of converter increases the effect on system can be noticed. Hence, adding of individual controllers will make the system more complex and costly. Hence, in [2], a nonideal resonant controller has been implemented to mitigate the circulating currents. Resonant controller has the capability to suppress the specific harmonic components but it fails to operate at higher order frequencies which may leads to instability of the system. In [11], a digital plug in repetitive controller with carrier phase shifted PWM has been proposed; which intended to eliminate higher and lower order harmonics. The disadvantage of that controller [11] is that it fails to operate at transient conditions and causes delay in fast response. Hence, in this article, an advanced digital robust repetitive controller paralleled with the PI controller has been implemented to reduce the harmonics up to 49th order.

B. Controller Design

The important requirement of the controller is to regulate the controlled variables to reference commands without any steady-state error against unknown disturbance input. To

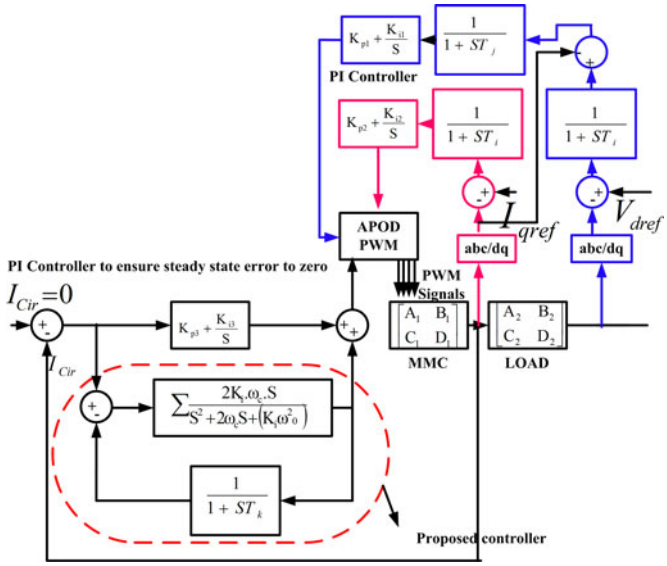

Fig. 6. Proposed harmonic controller applied to the MMC.

eliminate the steady-state error, one should use integral controller with its optimum gains. The unknown disturbance in this case is circulating currents for a fixed time period T. This proposed controller takes the input (circulating currents) from output terminals of the MMC and it acts as multiple harmonic controller. The complete block diagram of the controller with the MMC is shown in Fig. 6. The controller is paralleled with proportional (P) and integral (I) controller to obtain the better performance. The optimum values of P and I controllers are obtained with the use of the integral square error (ISE) technique. Where ω_c is the bandwidth, T_i is the measurement lag for voltage and current controllers, T_k is the measurement lag for harmonic controller, ω_o is the resonant frequency, K_p is the proportional gain, and K_i is the integral gain of the controller.

Primarily, the MMC and its resistive–inductive load has been modeled and denoted as

$$\begin{bmatrix} A_1 & B_1 \\ C_1 & D_1 \end{bmatrix} \begin{bmatrix} A_2 & B_2 \\ C_2 & D_2 \end{bmatrix},$$

respectively. The system has been employed with the current controller and voltage controller with inner integral current loop as shown in Fig. 5. For the voltage controller, the voltage at the terminals of load, which is in *a-b-c* form can be converted in to *d–q* form by using Park's Transformation technique. Thus, obtained results have been compared with the voltage reference wave (which is obtained through discrete virtual phase locked loop and resultant signal has been passed through the integral controller to ensure the steady-state error to zero. The same procedure has been implemented for current controller. The circulating currents from the terminals of the MMC have been compared with circulating current reference $I_{\rm cref}$ (in this case it is zero). Thus, obtained results have been passed through the proposed repetitive controller with parallel PI controller to ensure steady-state error to zero. The obtained signal decides the operative modulation index (MI) and subsequently the switching pattern of SMs. The values of the proportional and integral gains

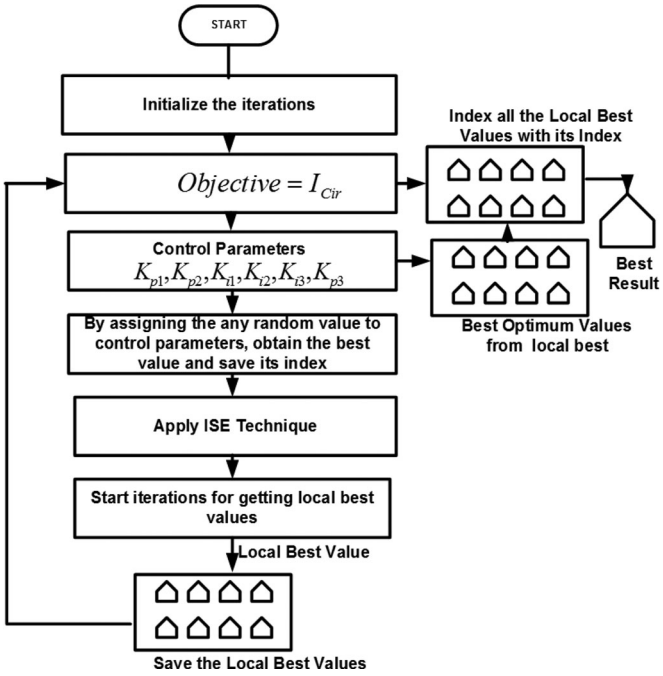

Fig. 7. Flowchart chart showing the applicability of ISE technique.

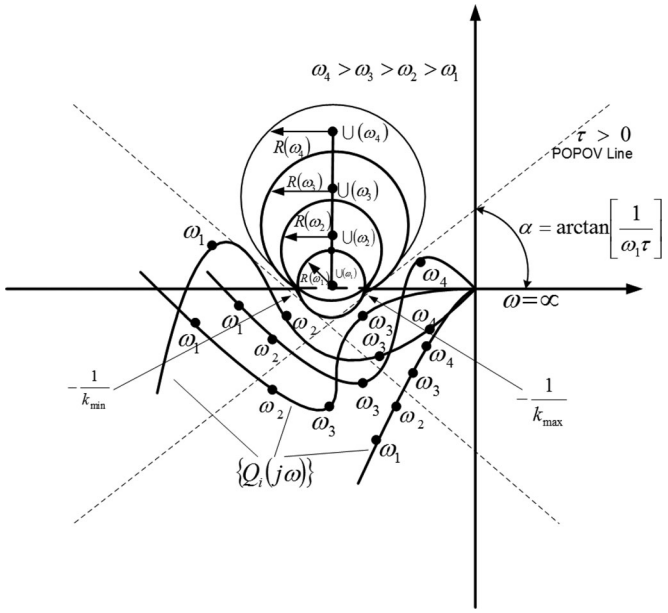

Fig. 8. Popov Stability analysis of a proposed controller.

have been obtained through the ISE technique. In this paper, the proportional and integral gains for all controllers have been considered as variables with circulating currents as an objective function. The detailed flowchart for the applicability of ISE technique have been shown in Fig. 7. The transfer function for the controller shown in Fig. 6 can be written by considering the following short equations as:

$$\frac{\omega_c \cdot s \cdot G_{rc}}{s^2 + 2 \cdot \omega_c \cdot s + \omega_0^2} = G(s)\frac{1}{R_r + s \cdot L_r} = L(s), \quad \left(\frac{1}{s \cdot (sT_k + 1)}\right) = H(s) \tag{28}$$

$$\frac{V_{\text{out}}}{V_{\text{in}}} = \frac{\left(K_p + \frac{K_i}{s}\right) + [G(s) + H(s)] \cdot L(s)}{1 + \left[\left(K_p + \frac{K_i}{s}\right) + \{G(s) + H(s)\} \cdot L(s)\right]}$$

$$V_{\text{out(cmd)}} - \frac{L(s) \cdot V_{\text{disturbance}}}{1 + \left[\left(K_p + \frac{K_i}{s}\right) + \{G(s) + H(s)\} \cdot L(s)\right]}. \tag{29}$$

Once the closed-loop controller is introduced in to the system, the stability of the controller will play a vital role. Since the system is nonlinear, hence, Popov's criteria is used to find its stability.

C. Stability Analysis by Using Popov Criteria

The system is said to be absolutely stable if it has a globally uniformly asymptotically stable equilibrium point at the origin for all nonlinearities in a given sector. The circle and Popov criteria give frequency-domain sufficient conditions for absolute stability in the form of strict positive realness of certain transfer functions. In the single-input-single-output case, both criteria can be applied graphically [14]. Popov criterion is used for stability analysis with nonlinear feedback system. There are some restrictions on using the Popov criterion. Popov criterion derives from the circle criterion and the scope application is smaller than Circle criterion. Popov criterion is restricted in the situation of $0 = \alpha < \beta$ which means that the graph of nonlinear system belongs to the sector [0, β]. Where α, β are Popov sector constants. The problem of nonlinear system stability can be solved by using Lyapunov stability analysis [14]. But the necessity of nonlinear system in state space, as Lyapunov method presumes, has restricted to certain extent its application in practice. Hence, Popov [14] criterion is applied to the system to investigate the stability of controller. The harmonic mitigated controller characteristic equation with unity negative unity feedback is expressed as T(s) in (30)

$$T(s) = \left[1 + \left(K_p + \frac{K_i}{s}\right) \cdot L(s)\right] \left[\frac{G(s) + \left(\frac{1}{sT_k + 1}\right)}{1 + \left(K_p + \frac{K_i}{s}\right) L(s)}\right] L(s). \tag{30}$$

As per Hurwitz criteria, the region of stability of the system is bounded by the values of the parameters α, β, at which both necessary and sufficient conditions of the asymptotic stability are satisfied. This region consists of the left lower quadrant bounded by the lines $\alpha < 1, \beta < 0$, and the right triangle with vertices $(0, 0), (1, 0), (1, 1)$. The resulting stability region is shown in the Fig. 8. Since the controller satisfies the Hurwitz criteria, it can move on to the testing stability of controller in various conditions. As per Popov criterion, the characteristic loci of T(s) do not circle the point $(\frac{1}{k_m\, in}, 0)$, but in the case of conditionally stable T(s), the total sum of anticlock wise encirclements of that point is equal to $m/2$, where m is the number of unstable poles of T(s). The transfer function T(s) should obeys the Popov's criteria only when the parameters $0 \leq (T_i(x)_i)/x_i \leq k_{\max} - k_{\min}$, where $i = 1, 2, 3 \ldots\ n, T_i(x)_i$ is the nonlinear elements in the system, $k_{\max}$ and $k_{\min}$ are the maximum and minimum limits

of the control system. To satisfy the stability condition of Popov criteria, the transformation matrix can be expressed in terms of canonical representation of Popov equations as

$$T_1(j\omega) = T(j\omega) \cdot \text{diag}\left[q_{Ti}(j\omega)\right] T^{-1}(j\omega) \tag{31}$$

where $q_T i(j\omega) = q_i(j\omega)/(1 + q_i(j\omega) \cdot k_{\min}; i = 1, 2, \ldots z$ are the stable canonical transfer functions of a transformed linear part, and $q_i(j\omega), T(j\omega)$ are the initial linear part of Popov matrix and canonical transfer function, respectively. Then, the complete representation of the transfer function can be represented as

$$T_2(j\omega) = T_1(j\omega) \cdot \text{diag}\left((1 + j\omega\tau)\frac{q_i(j\omega)}{1 + q_i(j\omega \cdot k_{\min})} + \frac{1}{k_{\max} - k_{\min}}\right) T^{-1}(j\omega). \tag{32}$$

The inequalities are not so convenient to use, hence, it adopts the absolute stability analysis to be conducted directly through the gain loci of T(s) of off circle criteria as shown in Fig. 8. The real parts of (31) can be represented as (32) for the satisfaction of Popov criterion

$$Re\left(q_i(j\omega) + \frac{k_{\max} + k_{\min}}{2k_{\max}k_{\min}}\right)^2 + lm\left(q_i(j\omega) + \omega_\tau \frac{k_{\max} + k_{\min}}{2k_{\max}k_{\min}}\right)^2 > R(\omega)^2 \tag{33}$$

where $R(\omega) = \frac{\sqrt{1+\omega^2\tau^2}}{2}(\frac{1}{k_{\min}} - \frac{1}{k_{\max}})$; $R(\omega)$ is the radius of the circle. The equation of circle in the complex plane of $T_i(j\omega)$, having its center at the point of $U(\omega)$ with coordinates as shown in (34) and (35)

$$lm\left(U(\omega)\right) + \frac{\omega_\tau}{2}\left(\frac{1}{k_{\min}} - \frac{1}{k_{\max}}\right) \tag{34}$$

$$Re\left(U(\omega)\right) + \frac{1}{2}\left(\frac{1}{k_{\min}} - \frac{1}{k_{\max}}\right). \tag{35}$$

Both $U(\omega), R(\omega)$ of the circle are functions of the frequency $'\omega'$ regardless its value and all circles intersect at real axis at the points $(1/k_{\min}, 1/k_{\max})$ as shown in Fig. 8. The angular coefficient of the tangents to the circles at these points are equal to $-1/\omega, 1/\omega_\tau$. These tangents of the point coincides with Popov Line $Re(T(\omega)) - \omega_\tau Im(T(\omega)) + 1/k_{\max} = 0$. For the Hermitian matrix $Re(T(\omega))$ to be positive definite at some frequency ω_n for a constant τ, it is necessary that Popov line is outside the circles and encirclements are not intersecting. Hence, the proposed controller is completely stable. The obtained values of $1/k_{\min}$ 2 and $1/k_{\max}$ is 5 with $1/\omega_\tau$ is 0.003. These values are obtained by substituting the necessary controller parameters in (31) and (32). It should be noted that the choice of controller parameters in the complex plane of Popov Criteria is not trivial. Hence, by observing the Fig. 8 and its graphical representation as shown in Fig. 9. The set of points at the loci $(T(\omega))$ marked by the frequency ω_n should be located at the outside of corresponding circle. The proposed controller stability analyzed with different conditions by plotting the magnitude and phase response as shown in Fig. 7(c). Primarily, the system is analyzed

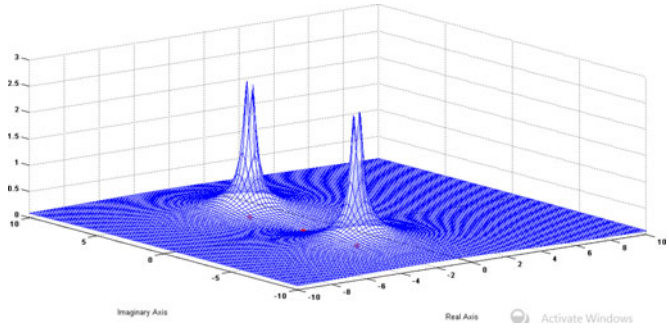

Fig. 9. Stability analysis for repetitive controller used for the MMC and its reaching criteria.

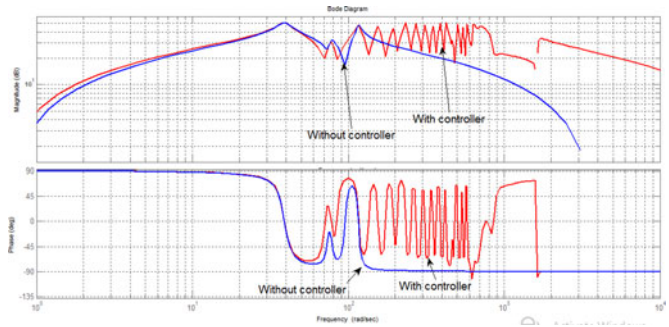

Fig. 10. Magnitude and phase response of repetitive controller used for MMC.

TABLE I
PARAMETERS IN THE MODELLING

Parameters	Symbol	Simulation, Experimental Values
Input voltages	V_{dc}	250 V
SM's Capacitance	C	16 mF-400 V
Arm Inductance	L	3 mH
Carrier frequency	F_c	1300 Hz
No. of SM's per arm	N	4
IGBT's	S	Inbuilt with resistance consideration/ FF600R07ME4-B11
Power Diode	D	Inbuilt with resistance consideration /RURG5060 50 A, 600 V Ultrafast Diode

without controller and then with controller. System without controller attenuates the harmonics at only certain periods, whereas with controller it attenuates for very large number of periods as shown in Fig. 10. From the graphical representation of the Popov approach, it is clear that system reaches steady-state stability.

IV. Simulated and Experimental Results

A down-scaled model of three-phase five-level MMC has been established to verify the proposed control system. The simulation and experimental parameters has been listed in Table I and controller parameters have been listed in Table II.

Fig. 11 shows a half-bridge circuit based on the MMC, where the stack number of chopper cells was selected as four per leg to confirm the basic operating principle, although the stack for HVDC systems will be used 47-level or more. Depending on the rating of the HVDC systems, the components of the systems will be selected. Fig. 11 shows that the experimental set-up

TABLE II
DOWNSCALED MODEL CONTROLLER PARAMETERS

Parameters	Symbol	Values
Controller	CONT	ATMEGA-16,16 MHZ 8 Bit Micro controller
Proportional gain	$K_{P1}K_{P2}K_{P3}$	3.14
Integral gain	$K_{I1}, K_{I2}K_{I3}$	2132
Stability Boundaries	$K_{\min}, K_{\max}$	(0.2,0.5)
Time constant	T_i, T_k	0.0002 S,0.0005S

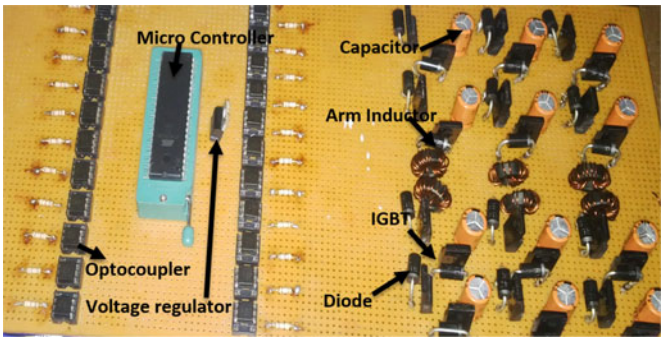

Fig. 11. Experimental setup of five-level MMC.

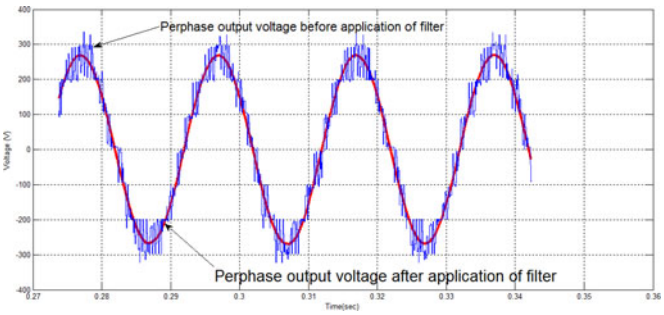

Fig. 12. Output voltage obtained through simulation.

of proposed MMC. All the components used for simulation and hardware have been shown in the Tables I and II. First, the MMC has been executed in Matlab/Simulink. The output voltage obtained from the simulation has been shown in Fig. 12 which is stepped sinusoidal signal without filter and smooth signal is observed after application of the LCL filter at the output terminals with voltage magnitude is 240 V (P-P). Fig. 13 shows the SM capacitor voltages for upper and lower SMs before and after application of controller. It consists of spikes and unbalances in the upper and lower modules before application of controller and spikes has been mitigated after application of controller. Also, there is increment in the output voltages as shown in Fig. 14. The system with controller is perfectly balanced and circulating currents are almost zero and is shown in Fig. 14. Also, the system has been examined for transient response for sudden change in its load. The proposed system was exposed to 10%, 20%, and 30% sudden change in loads and controller is able to attenuate the circulating currents perfectly and it is shown in Fig. 13. Without the controller, system is able to attenuate the harmonic components at 50 and 100 Hz. Whereas system with controller was able to attenuate the frequencies up to 2500 Hz. Hence, the

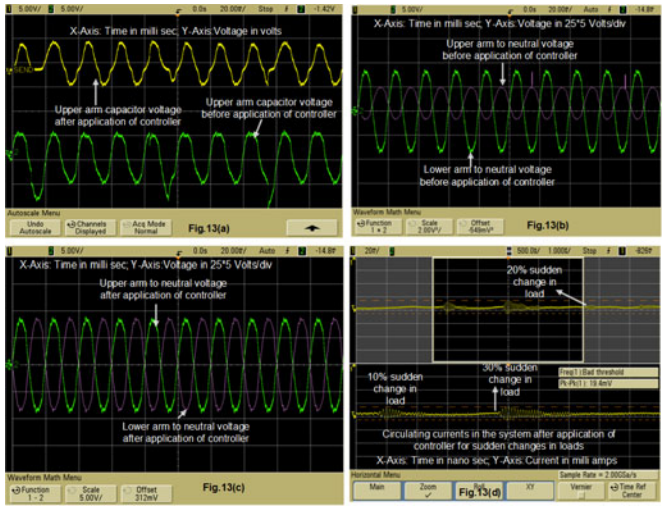

Fig. 13. Capacitor voltages, output voltage, output current and circulating currents obtained before and after application of controller.

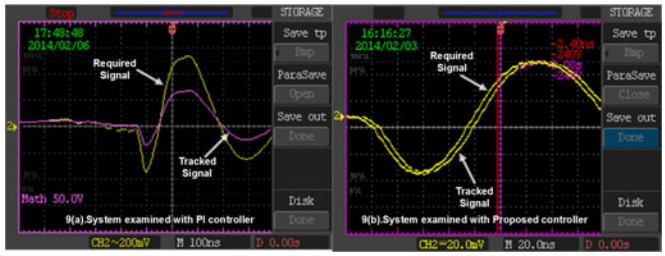

Fig. 14. Performance of proposed controller.

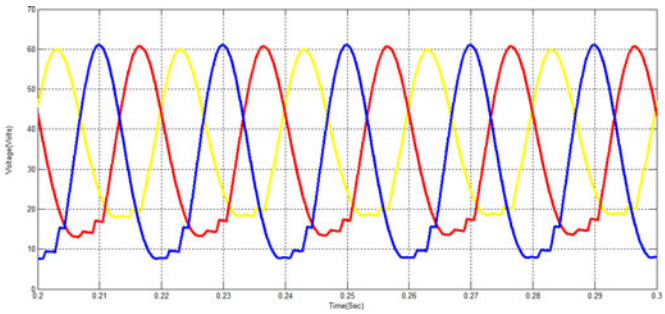

Fig. 15. SM capacitor voltages across R,Y,B phases of upper limb in the MMC.

system with repetitive controller gives better performance than system without controller. Also, it is observed that by changing the load, the performance of the controller remains unchanged. Without the application of controller to five-level MMC, the circulating currents passing through the legs of inverter is 2.0 A while the upper module and lower module capacitor voltages are fully unbalanced condition as shown in Fig. 14. Whereas after application of controller, the circulating currents reduced to 0.1 A with upper and lower modules are in balanced state which is shown in Fig. 14 and its voltage is 239.3 V with its current 4 A(P-P). Thus, it is proper that with the application of controller, the content of circulating currents has been reduced drastically. The performance of the controller for various disturbances and its tracking position is shown in Fig. 14 and voltage

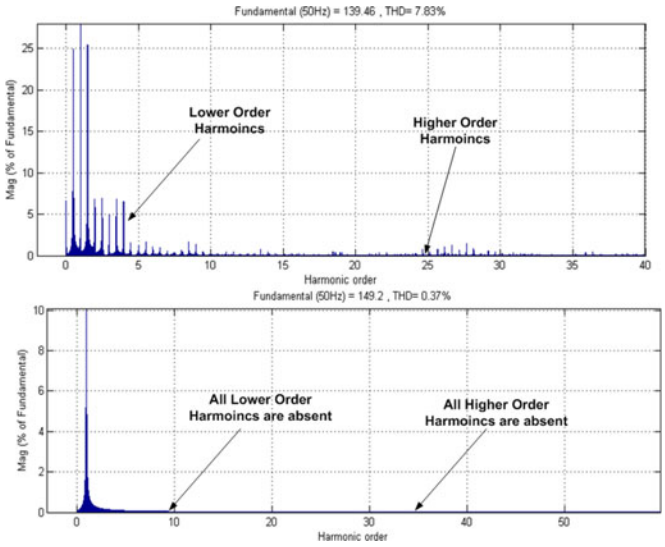

Fig. 16. Harmonic profile before and after application of controller.

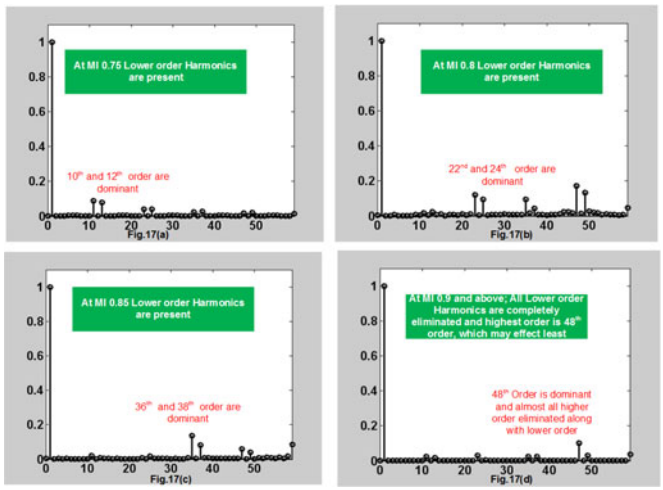

Fig. 17. Harmonic profile before and after application of controller.

across the SM capacitors is shown in Fig. 15. The system with PI controller is able to track the position with considerable delay and whereas with proposed controller, the system is able to track the required signal within 20 μs; which is quite acceptable for 50 Hz system. For any disturbance in the load, the controller reaches steady state in 10 μs and it follows the required path simultaneously without any delay. The THD performance is observed before and after application of controller. Before the application of controller, the fundamental peak amplitude is 136.46 with many number of lower and higher order harmonics. Whereas after the application of controller, the fundamental amplitude is 149.3 with zero lower order and higher order harmonics and is shown in Fig. 16. It achieves THD of 0.37% with controller, which is obtained with output LC filter and 7.83% of THD without controller. The experimental verification of harmonic profile with changing in the MI has been investigated and shown in Fig. 17(a)–(d). The system with 0.75 MI, the dominant harmonic components are 10th and 12th order; whereas with 0.8 MI, the dominant harmonics are 22nd and 24th order; whereas with 0.85 MI, the dominant harmonics are 36th and 38th order; whereas with 0.9 MI, the dominant harmonics are 48th order; thus it can be concluded that as the MI increases, the dominant harmonic components increase. The analysis consists of experimental verifications and simulations illustrate substantial decrement of THD to 0.37%. The removal of the filters in the output makes it less complicated and reduces the cost. This justifies the effectiveness of the proposed controller.

V. Conclusion

The second and other even-order harmonics in the circulating currents are mainly due to the fluctuations in the capacitor voltages in the SMs of MMC. This paper proposed an advanced repetitive controller to mitigate the circulating currents of the MMC. This method is simple and substantially eliminate the harmonic components with improved transient performance, while the voltages of SM capacitors are kept well balanced. This method is very helpful for real-time applications especially in the HVDC transmission systems. Both simulation and experimental results have shown the validity and effectiveness of the proposed method.

References

[1] M. Sreedhar, A. Dasgupta, and S. Mishra, "New harmonic mitigation scheme for modular multilevel converter: An experimental approach," *IET Power Electron.*, vol. 7, no. 12, pp. 3090–3100, Dec. 2014.

[2] S. Li, X. Wang, Z. Yao, T. Li, and Z. Peng, "Circulating current suppressing strategy for MMC-HVDC based on non-ideal proportional resonant controllers under unbalanced grid conditions," *IEEE Trans. Power Electron.*, vol. 30, no. 1, pp. 387–397, Jan. 2015.

[3] J.-W. Moon, J.-W. Park, D.-W. Kang, and J.-M. Kim, "A control method of HVDC-modular multilevel converter based on arm current under the unbalanced voltage condition," *IEEE Trans. Power Del.*, vol. 30, no. 2, pp. 529–536, Apr. 2015.

[4] G. Bergna, E. Berne, P. Egrot, P. Lefranc, A. Arzande, J.-C. Vannier, and M. Molinas, "An energy-based controller for HVDC modular multilevel converter in decoupled double synchronous reference frame for voltage oscillation reduction," *IEEE Trans. Ind. Electron.*, vol. 60, no. 6, pp. 2360–2371, Jun. 2013.

[5] Yalong Li and F. Wang, "Arm inductance selection principle for modular multilevel converters with circulating current suppressing control," in *Proc. 28th Annu. IEEE Appl. Power Electron. Conf. Expo.*, Mar. 17–21, 2013, pp. 1321–1325.

[6] Q. Tu, Z. Xu, and L. Xu, "Reduced switching-frequency modulation and circulating current suppression for modular multilevel converters," *IEEE Trans. Power Del.*, vol. 26, no. 3, pp. 2009–2017, Jul. 2011.

[7] Z. Li, P. Wang, Z. Chu, H. Zhu, Y. Luo, and Y. Li, "An inner current suppressing method for modular multilevel converters," *IEEE Trans. Power Electron.*, vol. 28, no. 11, pp. 4873–4879, Nov. 2013.

[8] G. Konstantinou, M. Ciobotaru, and V. Agelidis, "Selective harmonic elimination pulse-width modulation of modular multilevel converters," *IET Power Electron.*, vol. 6, no. 1, pp. 96–107, 2013.

[9] M. Zhang, L. Huang, W. Yao, and Z. Lu, "Circulating harmonic current elimination of a CPS-PWM-based modular multilevel converter with a plug-in repetitive controller," *IEEE Trans. Power Electron.*, vol. 29, no. 4, pp. 2083–2097, Apr. 2014.

[10] Q. Song, W. Liu, Z. Li, H. Rao, S. Xu, and L. Li, "A steady-state analysis method for a modular multilevel converter," *IEEE Trans. Power Electron.*, vol. 28, no. 8, pp. 3702–3713, Aug. 2013.

[11] L. He, K. Zhang, J. Xiong, and S. Fan, "Repetitive control scheme for harmonics suppression of circulating current in modular multilevel converters," *IEEE Trans. Power Electron.*, vol. 30, no. 1, pp. 471–481, Jan. 2015.

[12] D. C. Ludois and G. Venkataramanan, "Simplified terminal behavioral model for a modular multilevel converter," *IEEE Trans. Power Electron.*, vol. 29, no. 4, pp. 1622–1631, Apr. 2014.

[13] O. N. Gasparyan, *Linear and Non-Linear Multi Variable Feedback Controller: A Classical Approach*. New York, NY, USA: Wiley, 2008.
[14] M. A. Herrn, J. R. Fischer, S. A. Gonzlez, M. G. Judewicz, I. Carugati, and D. O. Carrica, "Repetitive control with adaptive sampling frequency for wind power generation systems," *IEEE J. Emerg. Sel. Topics Power Electron.*, vol. 2, no. 1, pp. 58–69, Mar. 2014.
[15] Y. Cho and J. Lai, "Digital plug-in repetitive controller for single-phase bridge less PFC converters," *IEEE Trans. Power Electron.*, vol. 28, no. 1, pp. 165–175, Jan. 2013.
[16] M. Sreedhar and A. Dasgupta, "Voltage balancing scheme in MMC-A new approach," *Int. J. Emerg. Elect. Power Syst.*, vol. 15, no. 4, pp. 389–399, Jul. 2014.
[17] K. Wang, Y. Li, Z. Zheng, and L. Xu, "Voltage fluctuation suppression method of floating capacitors in a new modular multilevel converter," in *Proc. IEEE Energy Convers. Congr. Expo.*, Sep. 17–22, 2011, pp. 2072–2078.
[18] E. Solas, G. Abad, J. A. Barrena, S. Aurtenetxea, A. Crcar, and L. Zajac, "Modular multilevel converter with different submodule concepts—Part I: Capacitor voltage balancing method," *IEEE Trans. Ind. Electron.*, vol. 60, no. 10, pp. 4525–4535, Oct. 2013.
[19] J. Mei, B. Xiao, K. Shen, L. M. Tolbert, and J. Y. Xheng, "Modular multilevel inverter with new modulation method and its application to photovoltaic grid-connected generator," *IEEE Trans. Power Electron.*, vol. 28, no. 11, pp. 5063–5073, Nov. 2013.
[20] F. Deng and Z. Chen, "A control method for voltage balancing in modular multilevel converters," *IEEE Trans. Power Electron.*, vol. 29, no. 1, pp. 66–76, Jan. 2014.
[21] P. Sai Prasanna, M. Sreedhar, and L. V. S. Kumar, "A review on circulating current suppression control, capacitor voltage balancing and fault analysis of modular multilevel converters," in *Proc. Int. Conf. Elect., Electron., Signals, Commun. Optim.*, Jan. 24–25, 2015, pp. 1–6.

Sreedhar Madichetty was born in Andhra Pradesh, India. He received the bachelor's degree in electrical engineering from Jawaharlal Nehru Technological University, Hyderabad, India, in 2010, and the master's degree in power electronics and drives from KIIT University, Bhubaneswar, India, in 2012. He received the Ph.D. degree in electrical engineering from KIIT University, India, in 2015.

He is currently with Birla Institute of Technology and Science Pilani, Pilani, India. His research interests include power electronics application in power system, power system stability and control, electrical machines, simulation and control of power system, renewable energy applications, and grid integration. He had authored 15 peer reviewed research articles.

Dr. Madichetty received the Medal for best performances in Masters and Scholatic Award for his research. He is a Member of Association of Computers, Electrical & Electronics Engineers, Indian Society for Technical Education, and International Association of Engineers.

Abhijit Dasgupta (M'13) received the Graduate degree in electrical engineering from Regional Engineering College, Durgapur, India (NIT, Durgapur), in 1977. He received the Post-Graduate degree in power electronics from IIT, Kanpur, India, in 1980.

He has worked in industry for 21 years. Since 2004, he has been a Professor with the School of Electrical Engineering, KIIT University, Bhubaneshwar, India. His research interests include power electronics, industrial electronics, digital control of electric drives, automatic generation control, and implementation of new optimization techniques.

Sambeet Mishra (S'13) was born in Odisha, India. He received the bachelor's degree in electrical engineering, and the master's degree with a specialization of power and energy system from KIIT University, in 2010 and 2013, respectively.

His research interests include the sphere of hybrid renewable energy system, power electronics, and soft computing application in power system.

Mr. Mishra is a Member of Institution of Engineers, India.

Chinmoy Kumar Panigrahi born on January 6, 1967, at Balasore, Orissa. He received the B.Tech. and M.Tech. degrees from Sambalpur University, Sambalpur, Orissa, India, in 1990 and 1997, respectively. He received the Ph.D. degree from Jadavpur University, Kolkata, West Bengal, India, in 2007.

He has a teaching experience of 20 years and research experience of 5 years. He is currently the Professor and Dean of the School of Electrical Engineering, KIIT University, Bhubaneswar, Odisha, India. His research interests include power system operation and control, renewable energy systems, and soft computing techniques. Six Ph.D. scholars obtained Ph.D. degree under his guidance and ten number of Scholars are working at present. He guided 32 M.Tech. Scholars till date. He has published many papers in referred journals and conferences.

Dr. Panigrahi is an Active Member of different professional society.

Ghouse Basha received the B.Tech. degree in electrical and electronics engineering, in 2010, and the M.Tech. degree in electrical power systems from Jawaharlal Nehru Technological University, Anantapur, Andhra Pradesh, India, in 2012.

He is currently an Assistant Professor in the Department of Electrical and Electronics Engineering, Annamacharya Institute of Technology and Sciences, Kadapa, Andhra Pradesh, India. His current research interests include power system planning and analysis, AGC, application of AI and power electronics to power system operation and control, and modular multilevel converters.